Boltzmann distribution in a nonequilibrium steady state: Measuring local potential by granular Brownian particles

Kiwing To*
Institute of Physics, Academia Sinica, Taipei, Taiwan 115, Republic of China
(Received 4 March 2014; published 9 June 2014)

We investigate experimentally the steady state motion of a millimeter-sized granular polyhedral object on vertically vibrating platforms of flat, conical, and parabolic surfaces. We find that the position distribution of the granular object is related to the shape of the platform, just like that of a Brownian particle trapped in a potential at equilibrium, even though the granular object is intrinsically not at equilibrium due to inelastic collisions with the platform. From the collision dynamics, we derive the Langevin equation which describes the motion of the object under an effective potential that equals the gravitational potential along the platform surface. The potential energy is found to agree with the equilibrium equipartition theorem while the kinetic energy does not. Furthermore, the granular temperature is found to be higher than the effective temperature associated with the average potential energy, suggesting the presence of heat transfer from the kinetic part to the potential part of the granular object.

DOI: 10.1103/PhysRevE.89.062111 PACS number(s): 05.70.Ln, 05.40.Jc, 05.20.−y, 47.57.Gc

The Boltzmann distribution, which relates the probability of finding an equilibrium system with a certain energy, is a central result from the theory of equilibrium statistical mechanics [1]. For example, for a colloidal particle trapped by an optical tweezer in a fluid of temperature T, the probability of finding the particle at position $\vec{r}$ is proportional to $e^{-\beta U(\vec{r})}$ with $U(\vec{r})$ being the potential due to the focused laser beam, $\beta^{-1} = k_B T$ the inverse temperature, and k_B the Boltzmann constant [2]. Hence a Brownian particle can be used to probe the local potential by examining its equilibrium position probability distribution. However, is this also true for a particle in a nonequilibrium steady state (NESS) instead of an equilibrium state [3,4]? Observations of Boltzmann [5–9] and non-Boltzmann [10–13] statistics in driven NESSs have been reported in the past. The key difference between an equilibrium state and a NESS is the presence of nonvanishing fluxes in the latter. For instance, to sustain a dissipative system in a NESS, energy has to be supplied from the environment to compensate the dissipation. If the system has more than one degree of freedom, there may be energy equipartition among different degrees of freedom [14]. Finding out how energy flows among different degrees of freedom in a NESS will help us to understand the physical behaviors of the system [15,16] and to predict whether or not the Boltzmann distribution and energy equipartition are valid.

In this paper, we report experimental studies of a dissipative system in a NESS—a granular object (millimeter-sized polyhedron) bouncing on a platform of different shapes. Since the contact force between a granular object (GO) and the platform is inelastic, the kinetic energy of the GO will be dissipated and it will eventually rest on the platform. If the platform performs vertical oscillations, the GO will oscillate vertically and it will also acquire horizontal motion from collisions. Because of the stochastic nature of collisions, the motion of the GO on the platform resembles that of a Brownian particle in two dimensions [17]. Our data show that the NESS position distribution of the GO is indeed related to its local potential, determined by the shape of the platform. We also find that the ratio between the potential and kinetic energies does not follow the prediction from the equilibrium equipartition theorem. The possibility of heat flow from kinetic energy to potential energy is discussed based on the measured granular temperature and the effective temperature associated with the averaged potential energy.

The experimental setup is shown in Fig. 1(a). A circular aluminum platform of radius $R = 150$ mm with a curved surface that is 10 mm deep is mounted on an electromagnetic vibration system (VR) which oscillates the platform sinusoidally up and down at 30 Hz and amplitude a. The equation of the platform with a conical surface [Fig. 1(d)] is given by $z = s_1 r$ with $s_1 = 1/15$ where z is the vertical position from the bottom of the platform and r is the radial distance from the platform center. Similarly the equation for the parabolic platform [Fig. 1(e)] is $z = s_2 r^2$ with $s_2 = \frac{10}{225}$ mm^{-1}. A GO, which is a regular Teflon tetrahedron of edges 10 mm and mass $m = 284$ mg, is put on the vibrating platform. Unlike a sphere, the tetrahedron, which has edges and corners with radius of curvature 0.3 mm, induces random forces during collision with the platform and eliminates the regular modes that exist for spherical objects [18]. A programmable fast camera (CA) is used to capture images [see Fig. 1(b)] from above. We program the fast camera to take 10 frames at 100 frames/s within each second for at least 3000 s. In this way, we capture dynamics in two different time scales: 0.01 s and 1 s. From each fast image sequence, we locate the position of the object by computer codes modified from standard image analysis software [19] and calculate the average position $\vec{r} = x\hat{x} + y\hat{y}$ and velocity $\vec{v} = v_x\hat{x} + v_y\hat{y}$ within a time interval of 0.1 s. Figures 1(f)– 1(h) show the positions of the tetrahedron on platforms of different shapes. They are evenly distributed for the flat platform while those for the conical and parabolic platforms concentrate around the center.

From the positions and their temporal changes, the velocity probability densities $P_s(v)$ with $v = v_x, v_y$ and the position probability densities $P_s(q)$ with $q = x, y$ for the tetrahedron moving on platforms with flat ($s = f$), conical ($s = c$), and parabolic ($s = p$) platforms are measured. The results in

*ericto@gate.sinica.edu.tw

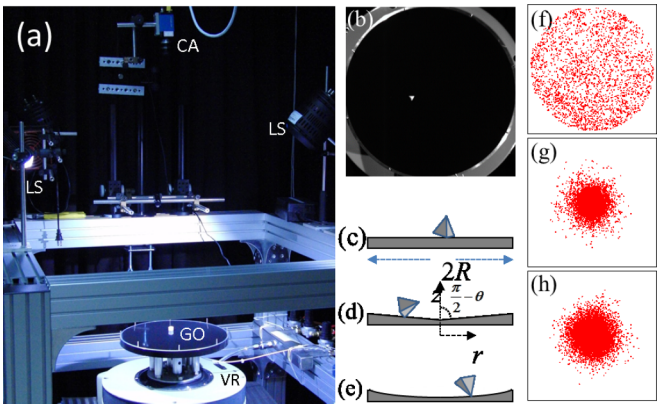

FIG. 1. (Color online) (a) Photograph of the experimental setup. (b) A typical image taken in the experiments. We perform experiments using platforms with (c) flat, (d) conical, and (e) parabolic surfaces. The positions of the GO are shown on (f) flat, (g) conical, and (h) parabolic surfaces. The physical dimensions of (f)–(h) are 150 × 150 mm^2.

Fig. 2(a) show that $P_s(v)$ in v_x and v_y are identical, as expected from symmetry. Furthermore, $P_s(v)$ on flat, conical, and parabolic platforms are similar to each other with their root-mean-square velocities $v_{\rm rms}$ increasing with vibration amplitude as shown in the inset. In fact when the velocities are scaled by $v_{\rm rms}$, the normalized probability densities $\mathcal{P}_s(v/v_{\rm rms})$

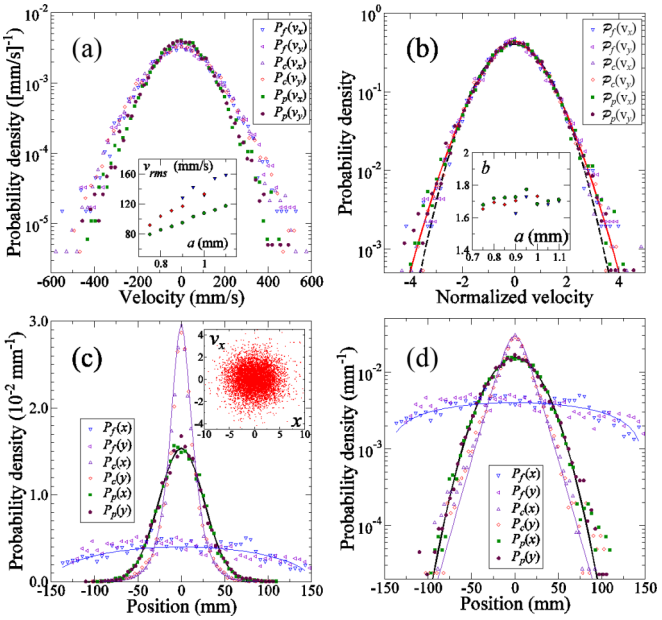

FIG. 2. (Color online) (a) Velocity probability densities $P_s(v)$ with $v = v_x, v_y$. (b) Velocity probability densities $\mathcal{P}_s(v/v_{\rm rms})$ normalized by the corresponding root-mean-square values $v_{\rm rms}$. Insets in (a) and (b) show, respectively, the $v_{\rm rms}$ and fitted stretched exponent b versus a for flat (blue ∇), conical (red ◇), and parabolic (green o) platforms. (c) Position probability densities $P_s(q)$ with $q = x, y$ for a tetrahedron on flat ($s = f$), conical ($s = c$), and parabolic ($s = p$) platforms. The inset is a scattered plot of v_x (0.1 m/s) versus x (10 mm) for the parabolic platform. (d) Same as (c) but on a semilogarithmic plot.

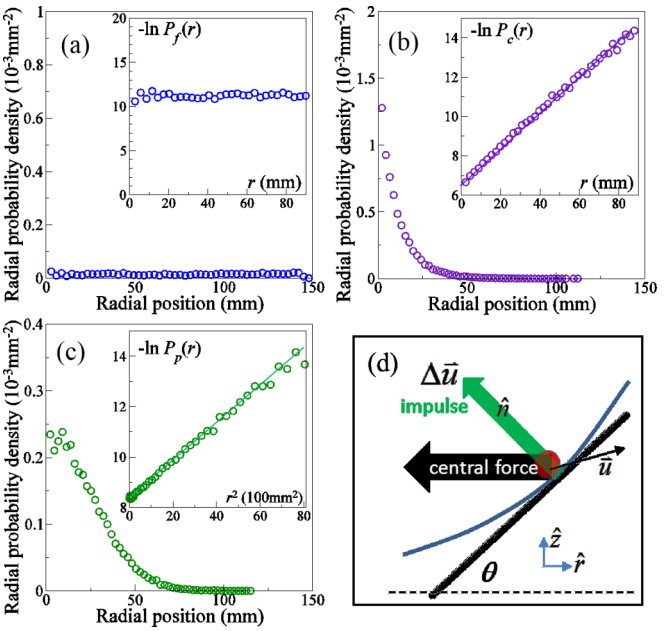

FIG. 3. (Color online) Radial probability density (RPD) for a tetrahedron on (a) flat, (b) conical, and (c) parabolic platforms. The insets show the negative natural logarithm of the RPDs. (d) Schematic diagram of collision dynamics.

collapse to a single curve as shown in Fig. 2(d). The black dashed curve in the figure is the best Gaussian fit to the collapsed data, suggesting that $P_s(v)$ are non-Gaussian. Nevertheless $\mathcal{P}_s(v/v_{\rm rms})$ can be fitted to a stretched exponential function $\exp(-A|v/v_{\rm rms}|^b)$ with $A = 0.68$ as indicated by the solid red curve. The inset shows that the stretched exponent b varies between 1.6 and 1.8 at different vibration amplitudes. In addition, there is no correlation between the velocity and the position as demonstrated from the inset of Fig. 2(c). Hence, the GO behaves like a *molecule* of a granular gas [15,20] in a nonequilibrium steady state.

Unlike the velocity probability densities, the position probability densities are qualitatively different for platforms of different shapes as shown in Figs. 2(c) and 2(d). They can be fitted to $P_f(x) \propto \sqrt{1-(x/R)^2}$ for the flat platform, $P_c(x) \propto \exp[-\sqrt{1+(x/x_o)^2}]$ with $x_o = 11.2$ mm for the conical platform, and $P_p(x) \propto \exp(-Bx^2)$ with $B = 7.4 \times 10^{-4}$ mm^{-2} for the parabolic platform. These density functions are, respectively, the expected forms for a uniform distribution, and distributions with linear dependence on the radial distance $r = \sqrt{x^2+y^2}$ from the center and with quadratic dependence on r. When the data are examined in polar coordinates (see Fig. 3), the radial distribution functions $P_s(r)$ ($s = f, c, p$ for flat, conical and parabolic platforms, respectively), which are the probability densities of finding the object at position r, confirm the r dependence of $P_s(r)$.

Since the GO appears to be attracted to the center except on the flat surface, an effective potential $U(r)$ should be present. To find the functional form of $U(r)$, we assume that the tetrahedron is at equilibrium with an effective temperature bath. Then $P_s(r)$ will be given by the Boltzmann distribution $P_s(r) = Ze^{-\beta U(r)}$ where β is the inverse temperature of the effective bath and $Z = (\int_0^\infty e^{-\beta U(r)} 2\pi r dr)^{-1}$ is the

normalization constant. So we have

$$U(r) = \ln Z - T \ln P_s(r), \tag{1}$$

where $T = \beta^{-1}$ is the effective temperature with k_B taken as 1. Therefore, the effective potential $U(r)$, when expressed in units of T, should have the same r dependence as $-\ln P_s(r)$ except for the addition of the constant $\ln Z$. The insets of Fig. 3 show the measured $-\ln P_s(r)$ for the flat, conical, and parabolic platforms, respectively. From symmetry arguments, it is not surprising to find that $-\ln P_s(r)$, and hence $U(r)$, is independent of r when the GO moves on the flat platform as shown in this figure. On the other hand, $U(r)$ for the conical platform increases linearly with r while that for the parabolic platform increases quadratically in r. The finding that the effective potential experienced by the GO follows the shape of the platform is also observed when the tetrahedron is replaced by a cube and at different vibration amplitudes.

It is possible to understand why the effective potential should follow the shape of the platform on which the GO moves. Consider a typical collision between the object and the platform surface as shown in Fig. 3(d). Let the velocity of the object before the collision be $\vec{u}$. The object receives an impulse that imposes a change in velocity $\Delta\vec{u}$ along the unit vector $\hat{n}$ normal to the surface at the point of contact. It is easy to show that $\Delta\vec{u} = -\lambda(\vec{u} - \vec{u}_b)\cdot\hat{n}\hat{n}$ where $\vec{u}_b$ is the velocity of the platform and $\lambda = (1+\alpha)$ with α being the restitution coefficient. (For elastic collisions, $\alpha = 1$ and $\lambda = 2$.) Then the component along the radial direction in the horizontal plane is

$$\begin{aligned}(\Delta\vec{u})_r &= -\lambda \sin^2\theta u_r + \lambda(u_z - a\omega \sin\omega t_i)\sin\theta\cos\theta \\ &\approx -\lambda \tan^2\theta u_r + \lambda(u_z - a\omega\sin\omega t_i)\tan\theta,\end{aligned} \tag{2}$$

where u_r and u_z are respectively the velocity components along the radial and vertical directions of the object; ω is the angular frequency of the platform oscillation; and t_i is the time of impact when the object hits the platform. Here we use the small-angle approximation such that $\sin\theta \approx \theta \approx \tan\theta$ which is the gradient $\kappa = dz/dr$ of the platform surface. Note that the quantities u_z and t_i are stochastic. In addition, the presence of corners and edges as well as the unknown angular momentum of the polygonal object contribute extra randomness ζ in the collision process. Hence, we have

$$\Delta u_r = -\lambda\kappa^2 u_r + \lambda(u_z - a\omega\sin\omega t_i)\kappa + \zeta. \tag{3}$$

Let the time between successive collisions be τ. This can be approximated by $\langle 2|u_z|\rangle/g$ with $g = 9.81$ m/s^2 as the acceleration due to gravity. Since the vertical velocity of the object at impact is mostly downward, we have $\langle u_z/|u_z|\rangle \approx -1$. Then the average acceleration is

$$\left\langle\frac{\Delta u_r}{\tau}\right\rangle \approx -\left\langle\frac{\lambda\kappa^2 u_r}{\tau}\right\rangle + \left\langle\frac{\lambda\kappa(u_z - a\omega\sin\omega t_i)}{\tau}\right\rangle + \left\langle\frac{\zeta}{\tau}\right\rangle,$$

which can be approximated to

$$\begin{aligned} m\frac{d\langle u_r\rangle}{dt} &= -\left\langle\frac{m\lambda\kappa^2 u_r}{2|u_z|/g}\right\rangle + \left\langle\frac{m\lambda\kappa u_z}{2|u_z|/g}\right\rangle + \left\langle\frac{m\zeta}{\tau}\right\rangle \\ &= -\left\langle\frac{\lambda mg}{|u_z|}\right\rangle\kappa^2\langle u_r\rangle - \frac{\lambda mg}{2}\frac{dz}{dr} + \left\langle\frac{m\zeta}{\tau}\right\rangle \\ &= -\gamma\langle u_r\rangle - \frac{dU_z}{dr} + \xi \end{aligned} \tag{4}$$

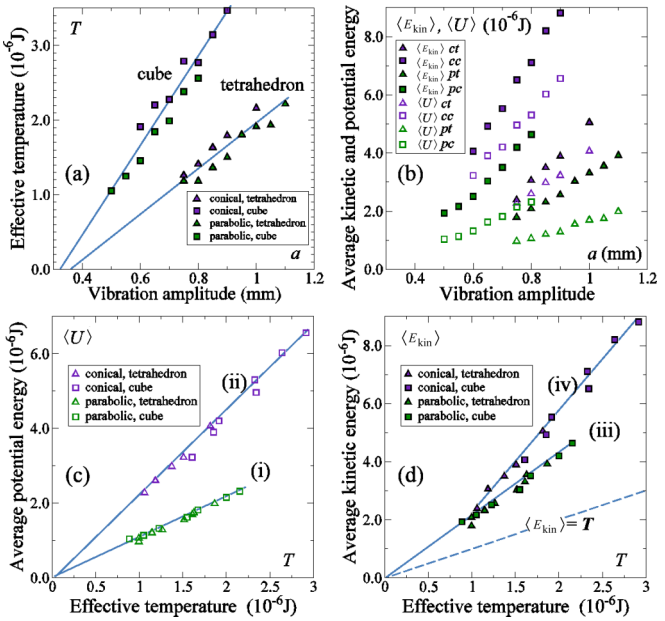

FIG. 4. (Color online) (a) Variation of effective temperature T with vibration amplitude a. (b) Variation of $\langle U\rangle_{ij}$ and $\langle E_{\rm kin}\rangle_{ij}$ with a. Here the subscript i (c for conical, p for parabolic) indicates the platform shape and j (t for tetrahedron, c for cube) represents the object shape. (c) Change of $\langle U\rangle$ with respect to T. (d) Change of $\langle E_{\rm kin}\rangle$ with respect to T.

with $\gamma = \langle\lambda mg\kappa^2/|u_z|\rangle$, $\xi = m\langle g\zeta/(2|u_z|)\rangle$, and $U_z = (\lambda/2)mgz$. This is a Langevin equation that describes the dynamics of an object moving with drag coefficient γ in a potential $U_z = (\lambda/2)mgz$. Since $z = s_\delta r^\delta$ for the conical ($\delta = 1$) and the parabolic ($\delta = 2$) platforms, the observed r dependence of the effective potentials $U(r)$ from the position distribution can be explained by setting $U(r) = U_z$.

The above analysis reveals how energy is supplied from the platform to sustain the motion of the GO. The stochastic force and the drag force act like a temperature bath that maintains the GO at effective temperature $T = \langle\xi^2\rangle/2\gamma$. Although evaluating T from $\langle\xi^2\rangle/2\gamma$ is difficult, T can be measured from the observed position distributions by matching the effective potential to the gravitational potential of the object along the platform surface. According to Eq. (1), the slope in the graph of $-\ln P_s(r)$ versus r^δ equals $(\lambda/2)mgs_\delta/T$, with $\delta = 1$ for the conical and 2 for the parabolic platform.

Figure 4(a) shows the measured T for the tetrahedron on conical and parabolic platforms at different vibration amplitudes a. Data for a Teflon cube of edge 5 mm and mass 254 mg are included for comparison. One can see that T increases linearly with a with a rate $\frac{dT}{da}$ which is higher for the cube than that for the tetrahedron. Presumably, a cube, which is more symmetric than a tetrahedron, has higher efficiency of converting the vertical motion to the horizontal motion than that of a tetrahedron. There is a threshold amplitude $\approx$0.37 mm at which the effective temperature vanishes. This threshold amplitude is about $1.5g$, which is approximately the acceleration needed to fluidized most granular packing [21].

In general, T is related to the energy $E = U + E_{\rm kin}$ in which the potential energy U and kinetic energy $E_{\rm kin}$ depend

on the position and velocity, respectively. Since the position and velocity are uncorrelated as illustrated by the inset of Fig. 2(c), $E_{\rm kin}$ and U should be independently populated [11]. Figure 4(b) indicates that their averages increase with a and their values ($\langle U\rangle$,$\langle E_{\rm kin}\rangle$) as well as their rates ($\frac{d\langle U\rangle}{da}$,$\frac{d\langle E_{\rm kin}\rangle}{da}$) are larger on the conical platform than on the parabolic platform. Note that the acquisition of energy in the horizontal plane from collision with the platform increases with the gradient $\kappa = \frac{dz}{dr}$. It is easy to show that the average gradient experienced by the GO on the conical platform is bigger than that on the parabolic platform in our experiment. Hence the conical platform is more effective in injecting energy to the GO than the parabolic platform, so that the energies of the GO on the conical platform are larger than those on the parabolic platform.

Quantitatively, the dependence of $\langle U\rangle$ and $\langle E_{\rm kin}\rangle$ on object and platform shapes is not obvious from Fig. 4(b). However, when they are plotted against T, they collapse onto four lines that depend only on the platform shape: $\langle U\rangle = C_U T$ with $C_U = 0.9$ and 2.0 for (i) parabolic and (ii) conical platforms [Fig. 4(c)]; together with (iii) $\langle E_{\rm kin}\rangle = C_K T$ with $C_K = 1.9$ for the parabolic platform and (iv) $\langle E_{\rm kin}\rangle = C_K T - 1.3 \times 10^{-6}$ J with $C_K = 3.0$ for the conical platform [Fig. 4(d)]. Considering the conservative nature of potential energy, it is not surprising to find that the measured values of C_U are consistent with the equilibrium energy partition theorem for linear ($C_U = 2$) and quadratic ($C_U = 1$) potentials [22]. On the other hand, kinetic energy, which decreases upon inelastic collisions, is not an equilibrium quantity. Hence, we do not expect the measured values of C_K to be equal to that predicted by equilibrium energy equipartition [14].

The GO is not at equilibrium because energy is needed to keep the object moving. When the motion is analyzed in the vertical and horizontal degrees of freedom separately, kinetic energy in the horizontal direction ($E_{\rm kin}$) is supplied to the GO by collision with the vertically moving platform. In between collisions, the effective potential energy (U) changes due to change in the horizontal position, while gravity increases or decreases the vertical velocity and hence sets the horizontal position and the vertical velocity at the next collision. Direct correlation between the fluctuations of $E_{\rm kin}$ and U should be absent due to the presence of randomness during collisions. Nevertheless, energy may flow between $E_{\rm kin}$ and U. Since $\langle E_{\rm kin}\rangle$ can be interpreted as the granular temperature T_g in our experiment [15,17,23], the fact that all the data points in Fig. 4(d) are above the line $\langle E_{\rm kin}\rangle = T$ implies $T_g > T$. In other words, the granular temperature is higher than the effective temperature which characterizes $\langle U\rangle$ and hence it is plausible that energy, in the form of heat, may flow from the kinetic part to the potential part. The existence and details of such heat flow will be investigated in the future.

To summarize, we have studied the dynamics of a polygonal object (a tetrahedron and a cube) moving on vertically vibrating platforms of different shapes. In the horizontal plane the object behaves like a Brownian particle under an effective potential that follows the shape of the platform surface. A simple theory based on collision dynamics is proposed to relate the observed potentials to the gravitational potential of the object along the surfaces. This result demonstrates the capability of a GO as a probe to measure the local potential from its position distribution in a nonequilibrium steady state. We also find that energy equipartition between the potential and kinetic parts is different from that predicted by the equilibrium equipartition theorem. In addition, the granular temperature is found to be higher than the effective temperature associated with the potential, suggesting the possibility of heat transfer from kinetic energy to the effective potential energy of the GO. These findings, when properly understood, will be useful in formulating a basic nonequilibrium steady state theory that is applicable to dissipative systems in general.

The author would like to thank J. C. Tsai, Professor D. Frenkel, and Professor S. Ramaswamy for their valuable comments and suggestions. This research is supported by the National Science Council of Taiwan under Grant No. NSC 102-2112-M-001-027-MY2.

[1] L. D. Landau and E. M. Lifshitz *Statistical Physics*, A Course of Theoretical Physics Vol. 5 (Pergamon Press, Oxford, 1969).
[2] G. M. Wang, E. M. Sevick, E. Mittag, D. J. Searles, and D. J. Evans, Phys. Rev. Lett. **89**, 050601 (2002).
[3] R. K. P. Zia and B. Schmittmann, J. Stat. Mech.: Theory Exp. (2007) P07012.
[4] U. Seifert, Rep. Prog. Phys. **75**, 126001 (2012).
[5] B. Pouligny, R. Malzbender, P. Ryan, and N. A. Clark, Phys. Rev. B **42**, 988 (1990).
[6] J. S. Olafsen and J. S. Urbach, Phys. Rev. Lett. **81**, 4369 (1998).
[7] K. Feitosa and N. Menon, Phys. Rev. Lett. **88**, 198301 (2002).
[8] G. W. Baxter and J. S. Olafsen, Nature (London) **425**, 680 (2003).
[9] P. M. Reis, R. A. Ingale, and M. D. Shattuck, Phys. Rev. E **75**, 051311 (2007).
[10] G. DAnna, P. Mayor, A. Barrat, V. Loreto, and F. Nori, Nature (London) **424**, 909 (2003).
[11] R. P. Ojha, P.-A. Lemieux, P. K. Dixon, A. J. Liu, and D. J. Durian, Nature (London) **427**, 521 (2004).
[12] R. P. Ojha, A. R. Abate, and D. J. Durian, Phys. Rev. E **71**, 016313 (2005).
[13] A. R. Abate and D. J. Durian, Phys. Rev E **72**, 031305 (2005).
[14] K. Nichol and K. E. Daniels, Phys. Rev. Lett. **108**, 018001 (2012).
[15] W. Chen and K. To, Phys. Rev. E **80**, 061305 (2009).
[16] G. Hu, Y. Li, M. Hou, and K. To, Phys. Rev. E **81**, 011305 (2010).
[17] A. Sarracino, D. Villamaina, G. Costantini, and A. Puglisi, J. Stat. Mech. (2010) P04013.
[18] J. J. Barroso, M. V. Carneiro, and E. E. N. Macau, Phys. Rev. E **79**, 026206 (2009).

[19] J. C. Crocker and D. G. Grier, J. Colloid Interface Sci. **179**, 298 (1996).
[20] J. S. van Zon and F. C. MacKintosh, Phys. Rev. Lett. **93**, 038001 (2004).
[21] P. Evesque and J. Rajchenbach, Phys. Rev. Lett. **62**, 44 (1989).
[22] R. C. Tolman, Phys. Rev. **11**, 261 (1918).
[23] A. R. Abate and D. J. Durian, Phys. Rev. Lett. **101**, 245701 (2008).